crystals

MDPI

Perspective

Plasmonic Modification of Epitaxial Nanostructures for the Development of a Highly Efficient SERS Platform

Ewa Dumiszewska [1], Aleksandra Michałowska [2], Libor Nozka [3,4], Dariusz Czolak [1] and Jan Krajczewski [2,*]

[1] Łukasiewicz—Institute of Microelectronics and Photonics, Al. Lotników 32/46, 02-668 Warsaw, Poland; ewa.dumiszewska@imif.lukasiewicz.gov.pl (E.D.); dariusz.czolak@imif.lukasiewicz.gov.pl (D.C.)
[2] Faculty of Chemistry, University of Warsaw, 1 Pasteur Str., 02-093 Warsaw, Poland
[3] Joint Laboratory of Optics of Palacky University and Institute of Physics AS CR, Institute of Physics of the Czech Academy of Sciences, 17. Listopadu 50a, 772 07 Olomouc, Czech Republic
[4] Joint Laboratory of Optics of Palacky University and Institute of Physics AS CR, Faculty of Science, Palacky University in Olomouc, 17. Listopadu 12, 771 46 Olomouc, Czech Republic
* Correspondence: jkrajczewski@chem.uw.edu.pl

Abstract: Epitaxy is the process of crystallization of monocrystalline layers and nanostructures on a crystalline substrate. It allows for the crystallization of various semiconductor layers on a finite quantity of semiconductor substrates, like GaAs, InP, GaP, InGaP, GaP, and many others. The growth of epitaxial heterostructures is very complicated and requires special conditions and the precise control of the growth temperature, the pressure in the reactor, and the flow of the precursors. It is used to grow epitaxial structures in lasers, diodes, detectors, photovoltaic structures, and so on. Semiconductors themselves are not suitable materials for application in surface-enhanced Raman spectroscopy (SERS) due to poor plasmonic properties in the UV/VIS range caused by missing free electrons in the conduction band due to the existing band gap. A plasmonic material is added on top of the nanostructured pattern, allowing for the formation of mixed photon–plasmon modes called localized surface plasmon-polaritons which stand behind the SERS effect. Typically, gold and silver are used as functional plasmonic layers. Such materials could be deposited via chemical or physical process. Attention has also been devoted to other plasmonic materials, like ones based on the nitrides of metals. The SERS performance of a functional surface depends both on the response of the plasmonic material and the morphology of the underlying semiconductor epitaxial layer. In the context of SERS, epitaxial growth allows for the fabrication of substrates with well-defined 3D nanostructures and enhanced electromagnetic properties. In this work, we described the possible potential plasmonic modification, composed of various coatings such as noble metals, TiN, and others, of well-developed epitaxial nanostructures for the construction of a new type of highly active SERS platforms. This abstract also highlights the role of epitaxial growth in advancing SERS, focusing on its principles, methods, and impact. Furthermore, this work outlines the potential of epitaxial growth to push the boundaries of SERS. The ability to design substrates with tailored plasmonic properties opens avenues for ultralow concentration detection.

Keywords: SERS spectroscopy; epitaxial growth; plasmonic nanostructures; nanoplatform

Citation: Dumiszewska, E.; Michałowska, A.; Nozka, L.; Czolak, D.; Krajczewski, J. Plasmonic Modification of Epitaxial Nanostructures for the Development of a Highly Efficient SERS Platform. *Crystals* **2023**, *13*, 1539. https://doi.org/10.3390/cryst13111539

Academic Editors: Stephanie Tomasulo and Aaron Ptak

Received: 29 September 2023
Revised: 20 October 2023
Accepted: 25 October 2023
Published: 26 October 2023

1. Introduction

1.1. Epitaxial Growth of Semiconducting Nanostructures

Nanostructures are typically formed via epitaxy using the MOVPE and the MBE methods. Depending on the precursors used, nanostructures with different elemental compositions can be formed. The applied method also allows for the formation of non-stoichiometric nanostructures. Depending on the reaction conditions, such as the temperature in the reactor, the nature of the precursor, the flow rate of the precursor, and the carrier gas used, nanostructures with different morphologies can be formed. Samples with

a well-defined structure are manufactured and the technology is repeatable from point to point and from sample to sample.

Nanowires are materials composed of one-dimensional nanostructures. They are ≥100 nm wide and 1000 times as long as they are wide. Due to the high aspect ratio of the nanowires, they have good thermal and electrical conductivity. The structure of nanowires is mainly composed of semiconductors, conductive polymers, and metal oxide components such as gold, copper, and silver [1].

During a typical vapor–liquid–solid (VLS) growth process, metal nanoparticles (NPs) are deposited on the substrate, acting as physical and chemical catalysts. Nanoparticles provide a physical location for incoming semiconductor reactants and facilitate their activation/decomposition. Gold is the most commonly used metal catalyst for VLS nanowire (NW) growth due to its chemical inertness and ability to form eutectic alloys and important semiconductor materials. The three main steps of VLS growth are I: metal alloying, II: nucleation, and III: NW growth [2]. The gold catalyst method is the most popular technique for growing semiconductor nanowires with the VLS method. It allows for fine control over nanowire morphology, density, position, and crystal structure [3]. Unfortunately, the VLS mechanism using Au catalysts may inadvertently incorporate impurities that affect the electronic and optical properties of the semiconductor grown [4].

During the epitaxial growth of nanostructures like nanowires, as the total pressure decreases, mass transport becomes faster and surface dynamics become dominant even in the moderate temperature range. This is because the average time between gas phase collisions increases with decreasing pressure, resulting in a diffusion coefficient that is inversely proportional to pressure. In this case, the growth process is completely heterogeneous. In the low temperature range, growth is limited by pyrolysis and the growth rate is lower. It has been observed that the flux of precursors affects the growth rate and, thus, the quality of nanostructures such as epitaxial nanowires. The precursor flow rate determines the precursor concentration in the reaction chamber, which affects the crystalline quality of the nanowires. When the precursor concentration is high, nanowires tend to have high defect densities, which limit the performance of nanowire-based devices [5].

1.2. Current Application of Epitaxial Semiconducting Nanostructures

With the use of effective carrier confinement in semiconductor nanowires in two dimensions and the excitation of radial and longitudinal optical modes, a wide range of applications and functions have been enabled [6]. Applications including sensing [7], photovoltaics [8], photo-detection [9], etc., have been demonstrated.

Advances in the growth of semiconductor nanostructures over the past two decades have stimulated tremendous scientific interest and research in the field of nanowire lasers [10]. As a result, nanowire lasers have been implemented on many different material platforms. The growth in nanowires has less stringent requirements for lattice matching with the growth substrate, and, due to stress relaxation, nanowires can have lower defect densities compared with bulk crystals [11–13]. The simple design is particularly noteworthy. Laser cavities using nanowires are compared with conventional planar semiconductor lasers, which require a large number of manufacturing steps. Lasers can be demonstrated in a variety of enhanced materials—such as metal oxides [14], chalcogenides [15], nitrides [16], III–V semiconductors [17], and, most recently, perovskites [18]. Furthermore, nanowires open up the possibility of three-dimensional architecture [19] and high-density integration beyond the possibilities of planar or top-down lithography.

Since nanowires are comparable in size to various biological and chemical molecules, they have been used as a means of sensitive and selective detection of biochemical reactions, including surface-bound reactions. In recent years, nanowires have been used as biosensors for detecting viruses, where nanowire biosensors have been functionalized with antibodies with high binding specificity to the target virus, affecting the conductivity of the nanowires [20]. Silicon nanowires (SiNWs) were used as biosensors for the rapid detection of dengue serotype 2 (DEN-2) by recognizing its reverse transcription polymerase

chain product (RT-PCR). This is accomplished by covalently binding peptide nucleic acid (PNA) to the SiNW surface. The bonding is verified by measuring the resistance change in the SiNWs before and after the bonding process. It was confirmed that the SiNW-based biosensor could detect amplicons at concentrations below 10 fM within 30 min [21].

2. Optical Properties of Chosen Semiconducting Nanostructures Formed via Epitaxial Method

The SERS behavior of a functional surface is driven by both its plasmonic properties and surface morphology. The plasmonic properties are well described by the spectral dependence of its relative electrical permittivity $\varepsilon(\lambda)$, which is called the dielectric function. For a given wavelength λ, the value of the dielectric function is a complex number, i.e.,

$$\varepsilon(\lambda) = \varepsilon_1(\lambda) + i\varepsilon_2(\lambda) \quad (1)$$

The dielectric functions of semiconductors in the UV/VIS region generally show complicated structures involving specific peaks whose positions depend, among others, on temperature, strain, grain size, and concentration of dopants. The structure reflects transitions between the valence and conduction bands (direct or indirect) of a given semiconductor separated by band gaps. Figure 1 summarizes separately real (ε_1) and imaginary (ε_2) parts of the discussed semiconductor materials. The imaginary part is related to the absorption of the material. Its decrease towards zero above a certain wavelength indicates a transition via photon absorption is not allowed below the corresponding energy of such photons due to the existing band gap.

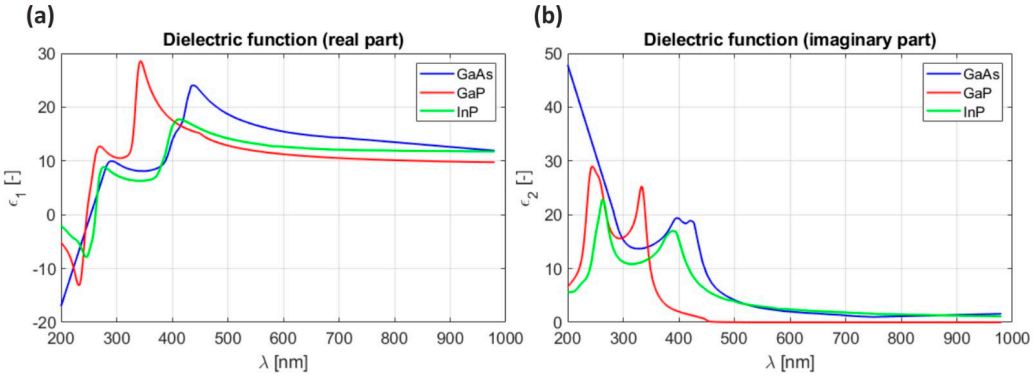

Figure 1. Typical dielectric functions (**a**) real part and (**b**) imaginary part of GaAs, GaP, and InP materials. Plots are prepared based on the dielectric constants available on https://refractiveindex.info/ (accessed on 29 September 2023).

The dielectric function describes optical properties, and hence it allows us to predict the possible SERS activity of various materials. One should note that the dielectric function is related to the material itself. Any conclusions concerning possible additional effects of the material morphology (texture and shape on the microscale and nanoscale) take optical constants into account.

When electromagnetic field oscillations (photons) enter a medium, they excite the internal states of that medium. The energy of these oscillations is shared between the electromagnetic wave and the internal excitations in medium. Such mixed modes are called polaritons (rather than photons). Depending on the photon energy, typically, lattice vibrations (phonons) are excited in the mid-infrared region, and bound electrons or free-plasma electrons are excited in the UV/VIS region. In the first case, mixed photon–phonon modes exist called phonon-polaritons, and exciton–polariton modes exist in the second case.

For SERS studies, mixed modes between free-plasma electrons and photons called plasmon-polaritons are the most relevant [22]. In the case of thin film surfaces (a metal film on a dielectric substrate), plasmons exist only in the presence of transverse electromagnetic waves (photons), resulting in the existence of propagating (or semi-propagating) surface

plasmon-polaritons (SPPs) [22]. However, by nature, the wave vector (and momentum) of propagating SPPs is always larger than that of the photon in the medium. Thus, the photon cannot directly excite an SPP. There are several techniques devised to impart the missing momentum, like Otto configuration [23] or Kretschmann configuration [24], on planar surfaces. Adding a morphology (texture) to the surface is another way to allow for the excitation of propagating SPPs. If the morphology is on the nanoscale (nanostructures) comparable to the wavelength of impacting light, the SPPs can exist for discrete energies (or wavelengths) only. These modes are then called localized surface plasmon-polaritons (LSPs) [22]. Due to stringent coupling conditions (conservation of momentum and energy), there are energies of incoming photons which are effectively transferred to the SPP or LSP modes. These modes are called surface plasmon resonances, which are the base of the SERS of the functional surface. Thus, the SERS activity for a given light wavelength is conditioned both by the plasmonic characteristics of the surface and its nanostructured morphology.

The requirement of the presence of free-plasma electrons in the SERS active medium implies metallic behavior for which $\varepsilon_1 < 0$ depending on the wavelength of the impacting light. Additionally, the optical absorption of the material must be small. As a rule of thumb, $20 \leq \varepsilon_1 \leq -1$ [22] and $\varepsilon_2 < 5$. Looking at Figure 1a, one can expect plasmonic properties of the presented semiconductors in the deep UV region (below 270 nm). There is, however, a higher absorption coefficient (125 μm^{-1} (1,250,000 cm^{-1}) at 200 nm for InP) compared with widely-used plasmonic metals like Ag (80 μm^{-1} (80,000 cm^{-1}) at 633 nm) or Au (68 μm^{-1} (680,000 cm^{-1}) at 633 nm).

Thus, the semiconductors are poor plasmonic materials. For SERS applications, they are used for the production of nanostructured substrates. An appropriate plasmonic metallic material is then deposited on top of them.

3. Plasmonic Functionalization

Because of the reason described in Section 3, pure epitaxial semiconducting nanostructures cannot be used as SERS platforms. However, the latest literature reports showed that such well-defined 3D nanostructures could be successfully used as patterns for modification by plasmonic nanostructures based on noble metal nanostructures or some other plasmonic materials, like TiN.

However, one should note that, at the moment, the application of semiconducting materials formed using the epitaxial method is related to their shapes and geometry, not to their chemical composition. The most important parameters are the homogenous distribution of nanostructures with the desired shape and size on the whole sample surface. Due to the fact that all the materials described do not possess plasmonic properties, the chemical composition does not play any role and surface plasmonic modification is needed.

The main advantage of epitaxial-formed semiconducting nanostructures in comparison with nanostructures formed via different chemical or physical methods is being well-ordered, repeatable structures with high homogeneity of well-defined nanostructures. Importantly, such nanostructures can be formed in reproducible ways in properly optimized conditions in special reactors. Some reports also showed good time stability of nanostructures after gold layer deposition. Therefore, one may believe that the development of an efficient modification method for semiconducting nanostructures formed via the epitaxial method with plasmonic nanostructures can play an important role in the development of novel, highly active, and sensitive SERS platforms.

3.1. Modification by Plasmonic Noble Metals

3.1.1. Modification by Plasmonic Noble Metal Nanoparticle Deposition

It is well known since the 1980s that noble metal nanoparticles can effectively enhance the Raman signal. The first reports about gold nanoparticle formation are related to the work of Turkyevich [25,26], and those about silver nanoparticles are described by Lee [27]. Both methods rely on chemical reduction of the metallic precursor ($HAuCl_4$ and $AgNO_3$, respectively) in a hot aqueous solution by an excess of citrate ions. The citrate ions play

dual roles as reducing agent as well as stabilizing agents. Many modifications of this method, like time, the temperature of the reaction, the reagent ratio, and so on, can lead to changes in the size of the formed nanoparticles. Nevertheless, in all cases the formed nanoparticles are spherical in shape.

The theoretical calculation supported by further experiments showed that the optical properties of noble metal plasmonic nanoparticles are strongly connected with the shape and size of nanostructures. Therefore, many chemical methods were reported to obtain noble metal nanoparticles with various shapes.

One of the most common methods is the so-called seed-mediated growth method. This method contains two parts. In the first part, small, spherical seeds are formed by the chemical reduction of gold ion precursor ($HAuCl_4$) via a reductor, typically sodium borohydride [28]. The formation of a red or brown solution after the addition of $NaBH_4$ indicates the formation of Au seeds. Because of their nature and small size, such seeds are unstable in time; however, a typical time before using a seed is in the range of 1–4 h. During this time, the decomposition of excess of $NaBH_4$ occurs. In the second step, a special growth solution is prepared. The solution contains a surfactant, mainly CTAB, CTAC, or a mixture, and the excess of the gold ion source. The influence of CTAB and CTAC on the final shape of formed nanoparticles is presented in Figure 2. Commonly, $AgNO_3$ and HCl are also added to ensure the desired nanoparticle-shape formation. The process starts after the addition of freshly prepared ascorbic acid (AA). The AA is too weak a reductor to reduce $HAuCl_4$ to its metallic form, but in the presence of Au seeds the reduction occurs on Au nanoparticles, which act as seeds for reduction and further growth. The time of the process depends on many factors, and it is in the range of 5 min even until overnight.

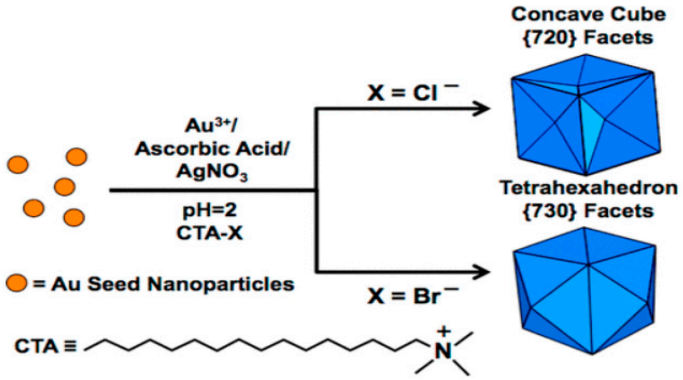

Figure 2. Diagram illustrating the seed-mediated growth method under specific conditions. Depending on the surfactant applied (CTAB or CTAC), gold nanoparticles of various geometries were obtained. Reprinted with permission from ref. [28]. Copyright 2012 American Chemical Society.

Au nanoparticles with various shapes are possible through the seed-mediated growth process, like stars [29], rods [30,31], triangles [32,33], bipyramids [29,34], cubes [35], or concave cubes [36]. Other methods of synthesis of anisotropic noble metal nanoparticles could be the polyol method (reduction of the metallic precursor in hot polyol organic solvent) [37,38], the photochemical method (photo reduction of the metallic precursor caused by light in excess of citrate ions) [39], the electrochemical method (reduction of the metallic precursor by applied potential) [40,41], or laser ablation from a solid target [42,43].

Colloids with noble metal nanoparticles can be simply drop-casted on the desired substrate. In the case of a flat unstructured surface, the so-called coffee ring effect could be observed [44]. In such situations, most of the nanoparticles are localized in the ring around the drop, while the drop interior is almost empty. This effect is undesirable due to the non-homogenous distribution of plasmonic material on the sample surface, which leads to a highly unstable measured Raman signal.

For this purpose, in some cases the sample or nanoparticle surface could be functionalized with special organic molecules called linkers. Linker molecules, due to their specific

construction, exhibit affinity to metallic and sample surfaces. Typical linker molecules are silans like (3-Aminopropyl)trimethoxysilane (APTMS) [45] and (3-Mercaptopropyl)trimethoxysilane (MPTMS) [46] or other organic molecules with various, specific functional groups like polyethylenimine (PEI) [47], dopamine [48], or common carbohydrates like glucose [49]. As an effect, sample surfaces are covered by plasmonic nanoparticles in a more homogenous way. However, in the case of a nanostructured surface, some literature reports showed that nano-roughness present on the sample surface highly limited the undesired coffee ring effect. The nanoparticles are "trapped" in the nano-roughness and do not migrate to the drop edge. Such approaches were present for TiO_2 nanotubes [50] and WO_3 nanopore arrays [51].

At the moment, the number of published manuscripts describing the application of epitaxially formed materials are highly limited. One of the most promising papers described the formation of GaP nanocones on a Zn-dopped GaP (111) substrate in the presence of Au nanoparticles [52]. The particle concentrations were described on 10^8 particles in 1 cm^2. The growth was carried out in an AIXTRON AIX 200 MOVPE reactor (Herzogenrath, Germany). First, the substrate was heated up to 650 °C for 13 min under a PH_3 and H_2 flow and total chamber pressure of 20 mbar. Due to the use of Au colloids, each nanocone has a Au nanoparticle sitting on the top. The nanocones were approximately 2.5 μm in height, and their average diameter dimensions were 600 nm at the base and 30 nm under the Au seed particle. The silver nanoparticles were deposited via the electroless metal deposition method based on the chemical reduction of silver nitrate by hydrofluoric acid. The reaction was carried out at 25 °C in 3, 5, and 7 min. It was observed that with increasing reaction times the average sizes of nanoparticles are bigger, but the number of nanoparticles is lower. Due to the fact that the electric potential was higher close to the tops of the nanocones, nanoparticles grew preferentially on the upper part of the nanocones, and their formation was less likely towards the substrate. Figure 3 shows SEM images of formed nanocones after the deposition of silver nanoparticles. The described system was applied to the sensing of a typical Raman reporter molecule, rhodamine 6G, but the authors do not refer to any EF or detection limit. In the next paper, a similar system was examined, and EF was determined on 10^6 towards R6G molecules [53]. The highest SERS activity was detected on the samples covered by the smallest Ag nanoparticles, due to fact of "hot-spot" formation in the gap between nanoparticles. In another paper, similar GaP nanostructures were decorated with a MoS_2 nanolayer via chemical and physical vapor deposition [54]. The Raman spectrum revealed the characteristic peaks for both the GaP and MoS_2 structures. These results indicate the fact that semiconducting, non-metallic materials could also be applied for the construction of optical sensor devices.

The nanopyramidal InGaN/GaN nanostructures were also tested as a template for SERS measurements [55]. The structures were grown on a (001) Si surface in an AIXTRON 200/4 RF reactor. Ammonia (NH_3), trimethylgallium, triethylgallium, and trimethylindium were used as the gas precursors. The reaction conditions varied in the range 580–1000 °C. The 7 nm Au nanoparticles were deposited on the surface using an e-beam evaporator. The R6 G dye molecules could still be detected even at a concentration of 10–10 M. The authors stated that such high enhancement occurred due to the fact that 2D nitride layers effectively concentrate electrons towards the SERS-active surface. Additionally, such a surface provides adjustable quantized energy levels, universally channeling resonance charges for CT and LSPR at the molecule/metal interface.

Also, the epitaxially formed semiconducting nanostructures could be modified by plasmonic noble metal nanoparticles using a simple drop-casting technique. One can assume that the presence of nanostructures can significantly decrease the coffee ring effect. Because of the well-defined shape of the nanostructures, the number of attached nanoparticles can be significant. This will lead to the formation of an SERS platform with high EF and good stability in point to point analysis. Unattached nanoparticles in aqueous or non-aqueous solvents could be prevented by the surface functionalization of semiconducting surfaces or noble metal plasmonic nanoparticles.

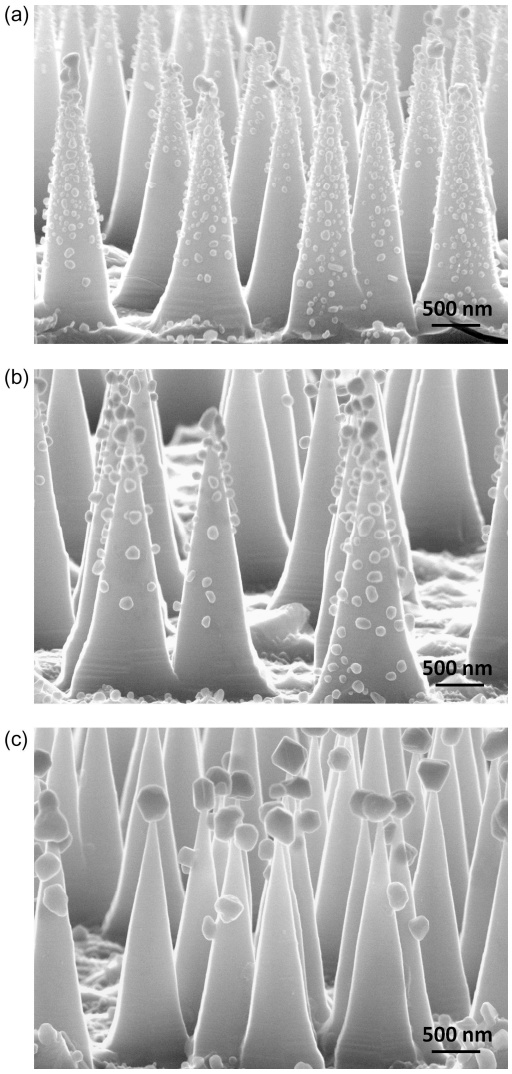

Figure 3. SEM images of GaP nanocones decorated with Ag nanoparticles via electroless chemical method from a $AgNO_3$ solution: (**a**) 3 min, (**b**) 5 min, and (**c**) 7 min of deposition. Reprinted with permission from ref. [52]. Copyright 2018 Elsevier.

3.1.2. Modification by Plasmonic Noble Metal Thin Film Deposition

There are several methods to coat substrates with plasmonic materials, and the choice of method depends on the specific application and the material being used. One of them is the modification of plasmonic metal deposition via Physical Vapor Deposition (PVD) [56]. There are various techniques in this method, such as sputtering, where a high-energy plasma is used to eject atoms or molecules from a plasmonic target material (typically Ag or Au), which are then deposited onto a substrate. The other variant of sputtering is magnetron sputtering, which uses a magnetic field to enhance the efficiency of ionization and improve film properties [57]. There is also evaporation-based PVD, where the plasmonic material is heated in a vacuum to create a vapor, and then condenses onto the substrate, forming a thin film [58]. The PVD method offers excellent control over the deposition process, which makes it valuable for applications where precise film properties are required. Due to the increased energy involved in sputtering, the obtained layers exhibit high packing density and good adhesion to the substrates [59]. On the other hand, there are limits in the homogeneity of such layers over the requested dimensions of the active surface areas which must be addressed, and their shape must be flat enough to avoid the existence of shaded areas on the surface.

Currently, there are a variety of metal targets, including Ag, Au, Cu, Ti, and others, allowing for the production of corresponding types of layers or their modifications, like TiN [55]. Above that, specialized geometric arrangements were studied for the direct production of nanostructured layers [59].

An optimal thickness of the metal layer depends on the dimensions of the nanostructures on the surface. For instance, a 70–120 nm thick Au layer was used for pyramidal silicon nanostructures a few micrometers in size in [22]. Very thin metal layers in order of a few tens of nanometers exhibit low SERS activity due to the low packing density of such thin layers. On the other side, thick layers tend to smooth sharp edges, corners, and tips of the nanostructure elements where the SERS activity is the most pronounced (hot-spots).

So far, authors have presented InP nanowires in only one report, formed using the epitaxial growth method and decorated by Au thin film with various thicknesses as the SERS active platform [60]. Nanowires were grown on an AIX 200/4 system using the MOCVD method on 20 × 20 mm InP (111) substrates with TMIn and PH_3 as indium and phosphorus precursors. Hydrogen was used as the carrier gas. The SEM and Raman analysis confirmed the formation of homogenously distributed InP nanowires. The average diameter of the InP nanowires was estimated to be 189.3 ± 9.3 nm for the top and 544.2 ± 45.9 nm for the base, while the length of the nanowires was ca. 800 nm. Such microstructures were covered by Au via magnetron sputtering under a constant current equal to 20 mA. The film thicknesses were controlled by the time. SEM cross-sectional images showed that the average thickness of the deposited Au film was 82.7 ± 7.0 nm for 3 min, 184.1 ± 7.7 nm for 5 min, and 221.4 ± 7.7 nm for 7 min. The described nanostructures are presented in Figure 4. Such a system was tested as an SERS platform for para-mercaptobenzoic acid (p-MBA). The recorded SERS exhibits two strong peaks located at 1077 cm^{-1} and 1587 cm^{-1}, which are due to the v_{12} and v_{8a} vibrations of the aromatic ring, respectively [61]. Based on the recorded spectra, the enhancement factor (EF) was calculated. It was found that the EF increased with the increasing thickness of the deposited Au film. For the thickest layer, the EF reached 2.26 × 10^6. Such a high EF is, to the best of our knowledge, one of the highest SERS enhancement factors for gold-based SERS platforms so far.

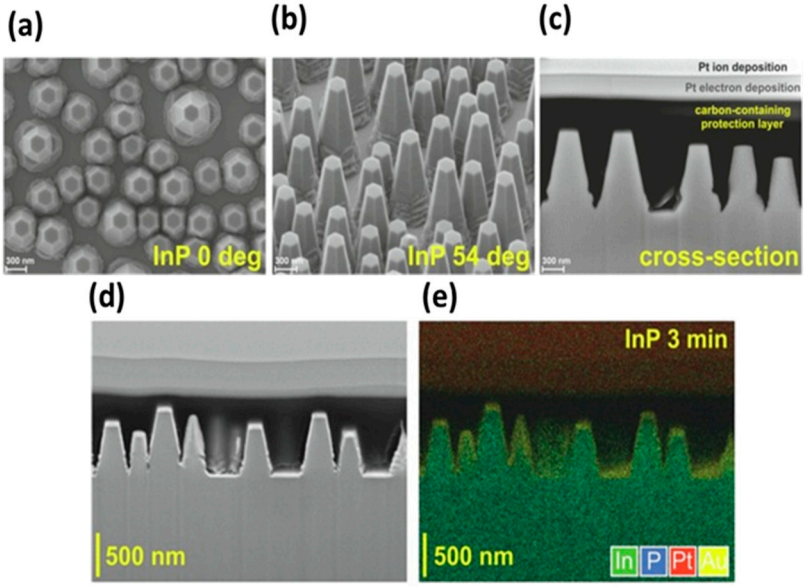

Figure 4. (**a**–**c**) SEM images of the InP nanowires under (**a**) 0° and (**b**) 54°, (**c**) a cross-section image of the InP nanowires. (**d**,**e**) FIB cross-sectional images of the Au@InP nanowires coated by Au thickness of 82 ± 7 nm. Reprinted with permission from ref. [61]. Copyright 2023 Elsevier.

Plasmonic materials can also be deposited using Chemical Vapor Deposition (CVD) techniques. The principle of this method is to control the chemical reactions between gaseous precursors in a high-temperature environment, in this case, noble metals. As

plasmonic precursors are introduced into a reaction chamber and exposed to heat, they decompose. Subsequently, the resultant species adsorb into the substrate surface, where they react and form a solid film [62,63].

Sometimes, in order to improve the solid properties of the sputtered plasmonic layer, obtained using the methods described above, the post-fabrication optimization of a substrate with film is applied. One of the methods used for this purpose is Rapid Thermal Annealing (RTA). The RTA process involves the rapid heating of the plasmonic thin-film metal layer to specific temperatures, typically in the range of 100 °C to 1000 °C, and for a short time, often from seconds to minutes [64,65]. After this process, cracked plasmonic films are obtained or, often, circular nanoparticles are formed; a scheme of this process and SEM images are presented in Figure 5. The key principle behind RTA is to induce structural and compositional changes in the plasmonic materials by exploiting the thermal energy to improve their optical properties.

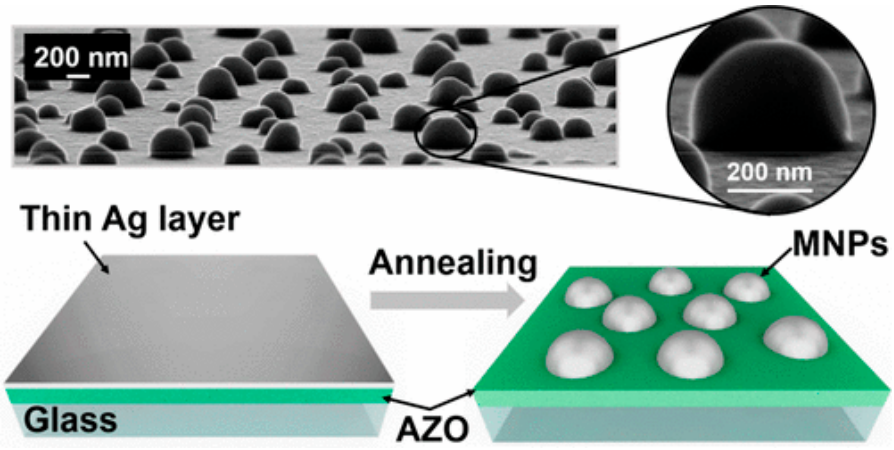

Figure 5. SEM micrograph and schematic illustration of rapid thermal annealing process. Reprinted with permission from ref. [65]. Copyright 2016 American Chemical Society.

A method that does not require post-fabrication optimization and immediately allows the formation of rough coatings is thermal spraying [66]. The process involves the deposition of a plasmonic material onto a substrate by heating it to a molten or semi-molten state and propelling it onto a surface, where rough surfaces, porous structures, and micro/nanoparticles can form. Thermal spraying can provide good reproducibility with proper process control of an SERS substrate with layers deposited in such a way.

3.2. Modification by Plasmonic Non-Metallic Nanostructures

Traditional plasmonic materials like gold and silver are well known for the ability to support surface plasmon resonances, which amplify interactions between light and matter, but non-metallic nanostructures also present unique benefits and are garnering interest in the context of surface-enhanced Raman spectroscopy (SERS) applications.

One of the most typical non-metallic plasmonic materials is titanium nitride (TiN), which is becoming more and more widely used for SERS [22,67–70]; currently, TiN nanostructures are mainly applied in photocatalysis. The high photocatalytic activity comes from the specific optical properties. The same optical properties could be responsible for SERS signal amplification.

TiN layers are prepared using various techniques, such as with metallic plasmonic films, usually physical vapor deposition, and especially magnetron sputtering [22,69,71]. Nanoparticles are also made of titanium nitride and the plasmonic properties of TiN nanoparticles can be tailored by adjusting their size, shape, and composition [72].

One possible way is using the so-called glancing angle deposition (GLAD) [64]. In this process, the substrate is not placed horizontally but at a certain angle relative to this orientation. As a result, nanostructures of various morphologies can be obtained. Figure 6

shows SEM images of the nanostructures formed. Most of the proposed syntheses of TiN nanostructures are based on physical process like sputtering or direct nitrification of previously obtained TiO_2 nanostructures [73,74]. But there is still a lack of rapid, efficient, and simple chemical methods for TiN nanostructure formation. Titanium nitride is known for its chemical stability, as it is resistant to oxidation and corrosion, which means that an SERS substrate with a TiN layer remains effective over extended periods, compared with, for example, a silver substrate [75,76]. This is significant because stability plays a critical role in ensuring consistent and reliable SERS measurements. It is believed that other metals belonging to the titanium group, like zirconium (ZrN) and hafnium (HfN) nitride, could also been used as highly efficient nanostructures for SERS.

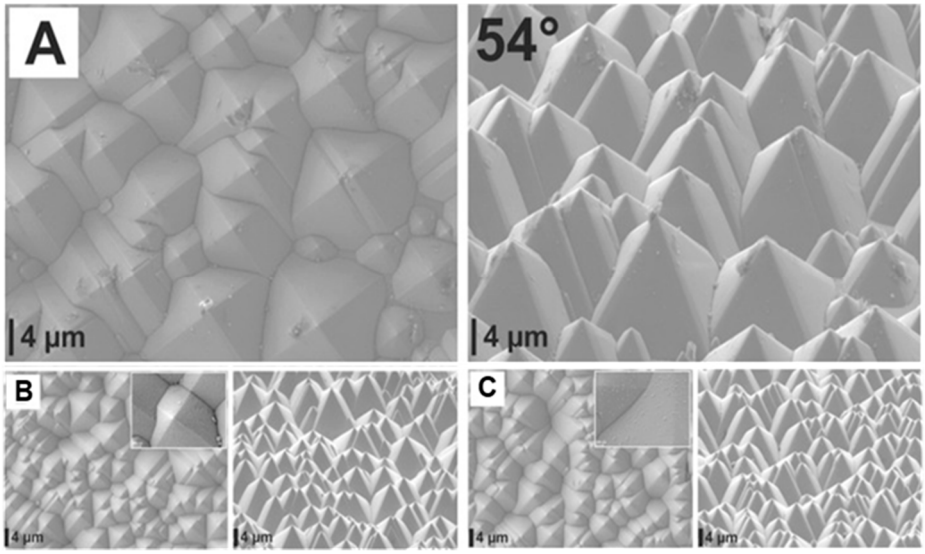

Figure 6. SEM images of Si pyramids: (**A**) unmodified Si pyramids formed via chemical etching in specific alkaline conditions under proper time and temperature; (**B**) covered with 80 nm of Au layer, 0 and 54° stage tilt; and (**C**) covered with 80 nm of TiN layer, 0 and 54° stage tilt. Reprinted with permission from ref. [22]. Copyright 2023 Elsevier.

As described above, many scientific groups all around the world are looking for effective preparation methods of XN nanostructures with various shapes. So far, there is only one report in which TiN and Au film deposited on nanostructures with the same morphology were compared in the field of optical properties and SERS activity. SEM images of Si nanopyramids and Si nanopyramids coated with Au and TiN layers with the same thicknesses are presented in Figure 7. The data analysis showed big similarities between the optical response of both material in the visible range. In the case of TiN thin film, an additional peak related in the UV range could be observed, which could be assigned to a band gap transition typical for semiconducting materials. The SERS analysis showed that both materials exhibit similar SERS activity with the limit of detection (LOD) in the range 10^{-9} M for the common dye molecule of tartazine.

Among various materials used for SERS substrates, molybdenum trioxide (MoO_3) and other MoO_{3-x} structures found potential applications in SERS [77–79]. MoO_3 is a transition metal oxide with a layered crystal structure, it exhibits interesting electronic and optical properties, and it can be synthesized in various nanostructured forms, such as nanowires, nanosheets, or nanoparticles [79–81]. As with other structures, the optical properties of molybdenum oxide structures can be tuned by controlling the morphology and size. It is proved that the localized surface plasmon resonance of molybdenum oxide structure nanostructures can significantly amplify Raman scattering signals from nearby molecules. For example, promising materials based on molybdenum oxides, MoS_2/MoO_{3-x} nanosheets, exhibit an EF estimated at 10^6, which allows for the detection of molecules

even in 10^{-9} M concentrations [78], while MoO_{3-x} microrods and nanobelts give EFs equal to 6.99×10^5 [79].

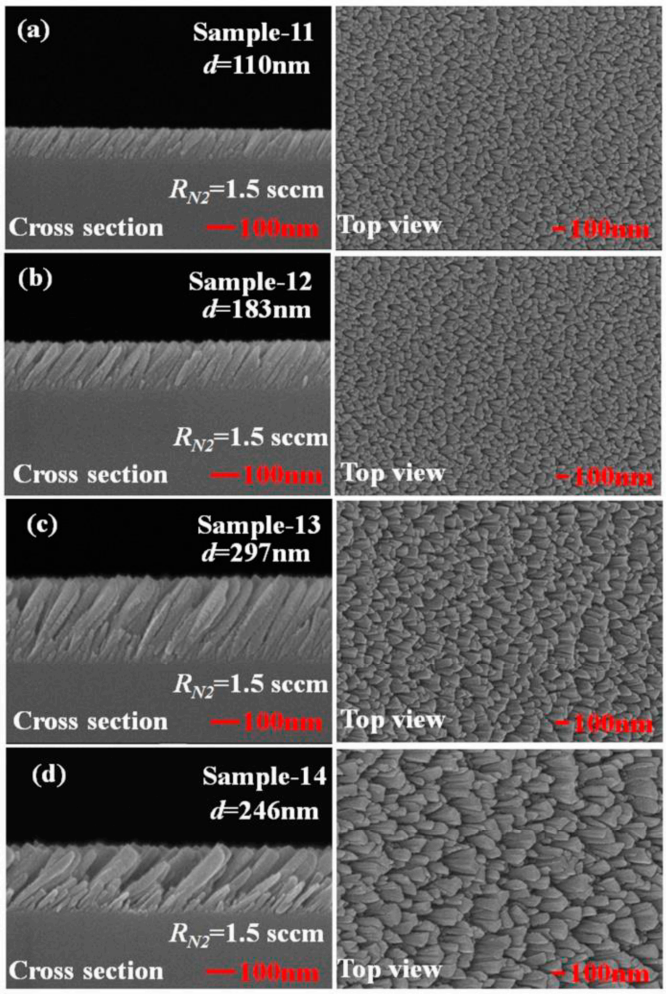

Figure 7. Cross-section and top view of SEM images of TiN nanorod arrays with different thicknesses (**a**) 110 nm, (**b**) 183 nm, (**c**) 297 nm, and (**d**) 246 nm. Reprinted with permission from ref. [68]. Creative Commons Attribution (CC BY) license.

Another non-metallic material showing plasmonic properties and potential application in the SERS technique is tungsten(VI) oxide (WO_3/ WO_{3-x}). WO_3 thin films on a solid template or formed nanostructure exhibit promising optical properties [82]. Although WO_3 does not possess the typical noble metal characteristics and strong plasmonic properties like gold or silver nanostructures, it can exhibit localized surface plasmon resonances (LSPRs) when engineered into specific nanostructures [83–85], and can be optimized by controlling its morphology, size, and crystal structure. This material is characterized by its electrochromic behavior, which means its optical properties change in response to an applied electric field; so, to enhance the signal in SERS, it can be obtained by changing the material's optical properties upon excitation with a Raman laser. The surface chemistry of WO_3 can perform strong adsorption and chemical interactions with analyte molecules which also lead to enhanced SERS signals. Just as importantly, tungsten trioxide is stable under various environmental conditions, which makes it possible to be used as a long-term SERS surface. To conclude, tungsten(VI) oxide-based nanostructures are a promising alternative for Raman signal amplification and could contribute to the development of more versatile SERS substrates. However, so far, SERS measurements are usually made using combinations of this oxide with silver or gold nanoparticles [51,86–88]. Hollow WO_3 nanospheres showed high SERS activity; the EF was estimated to be 1.6×10^6 [83],

while decorating WO_3 nanoflakes with silver nanoparticles allows for the increase in EF to 3.9×10^8, which corresponds to a 10^{-10} M detection limit [86].

In conclusion, one can assume that all of the semiconducting nanomaterials listed above could be deposited on epitaxial nanostructures for the construction of a novel class of SERS platform. Soon, this will allow for the rise of a new class of metal-free and efficient surfaces for SERS analysis. The main challenge to overcome is the development of a repeatable method of synthesis of both materials, homogenous distribution all around the surface, as well as time and chemical stability.

4. Conclusions

To fabricate highly effective SERS substrates, various methods and materials can be employed and some advice for the fabrication of such templates is universal and versatile. The size and shape of nanomaterials have a profound impact on the amplification in SERS; those structures with sharp edges clearly provide higher enhancement factors in measurements. Concerning the plasmonic properties of a material, it is necessary to ensure that the plasmonic resonance of the substrate matches the excitation laser wavelength used in Raman spectroscopy. For better results, one can combine noble metal nanoparticles with semiconducting materials and achieve synergistic effects. The choice of a substrate for SERS measurements depends on its ability to generate strong electromagnetic field enhancements and chemical interactions with the target molecules. Therefore, it is essential for SERS experiments to characterize and refine the fabrication methods to achieve the best results for a particular application. For instance, gold-modified structures are preferred in biochemical and biomedical analysis due to their better biocompatibility with good time stability. On the other hand, silver structures typically offer higher EFs. It is believed that in the future non-metallic plasmonic nanomaterials will also be widely used due to their promising optical properties. SERS is the one of the fastest developed analytical techniques based on plasmonic nanomaterials. Current achievements allow for the detection of trace amounts of organic molecules and, in some cases, even for single-molecule detection. Further development of the SERS method is possibly connected with the construction of novel plasmonic nanomaterials with improved properties. The epitaxial growth method allows for the formation of a well-defined structure on the nanoscale which is repeatable from point to point and from sample to sample. Due to their optical properties, such materials are so far mainly used in photovoltaic and related fields. However, we strongly believe that the surface modification of semiconducting nanostructures formed using the epitaxial method can offer a new class of nanomaterials with improved optical and structural properties. Such refinement will be associated with the formation of a novel class of SERS platform with extremely high EFs with good time and chemical stability. To date, most manuscripts report on plasmonic metal modification. It is strongly believed that, presently, non-metallic plasmonic structures obtained using the epitaxial growth method will ensure the development of a widely used SERS platform with improved properties.

Author Contributions: Conceptualization, J.K.; writing—original draft preparation, E.D., A.M., L.N., D.C. and J.K.; writing—review and editing, E.D., A.M., L.N., D.C. and J.K.; visualization, J.K., A.M., L.N., E.D. and D.C.; supervision, J.K.; project administration, J.K.; funding acquisition, J.K. and L.N. All authors have read and agreed to the published version of the manuscript.

Funding: L.N. gratefully acknowledges the support from Palacky University IGA PrF 2023_005. J.K. thanks the University of Warsaw, Faculty of Chemistry for its financial support.

Data Availability Statement: Not applicable.

Conflicts of Interest: The authors declare no conflict of interest.

References

1. Jatoi, A.S.; Ahmed Khan, F.S.; Mazari, S.A.; Mubarak, N.M.; Abro, R.; Ahmed, J.; Ahmed, M.; Baloch, H.; Sabzoi, N. Current Applications of Smart Nanotextiles and Future Trends. In *Nanosensors and Nanodevices for Smart Multifunctional Textiles*; Elsevier: Amsterdam, The Netherlands, 2021; pp. 343–365. [CrossRef]
2. Wu, Y.; Yang, P. Direct Observation of Vapor−Liquid−Solid Nanowire Growth. *J. Am. Chem. Soc.* **2001**, *123*, 3165–3166. [CrossRef]
3. Li, A.; Zou, J.; Han, X. Growth of III-V Semiconductor Nanowires and Their Heterostructures. *Sci. China Mater.* **2016**, *59*, 51–91. [CrossRef]
4. Noor Mohammad, S. Why Self-Catalyzed Nanowires Are Most Suitable for Large-Scale Hierarchical Integrated Designs of Nanowire Nanoelectronics. *J. Appl. Phys.* **2011**, *110*, 084310. [CrossRef]
5. Johnson, N.J.J.; Korinek, A.; Dong, C.; van Veggel, F.C.J.M. Self-Focusing by Ostwald Ripening: A Strategy for Layer-by-Layer Epitaxial Growth on Upconverting Nanocrystals. *J. Am. Chem. Soc.* **2012**, *134*, 11068–11071. [CrossRef] [PubMed]
6. Lu, W.; Lieber, C.M. Semiconductor Nanowires. *J. Phys. D Appl. Phys.* **2006**, *39*, R387–R406. [CrossRef]
7. Meng, J.; Li, Z. Schottky-Contacted Nanowire Sensors. *Adv. Mater.* **2020**, *32*, e2000130. [CrossRef]
8. Chen, Y.; Hrachowina, L.; Barrigon, E.; Beech, J.P.; Alcer, D.; Lyttleton, R.; Jam, R.J.; Samuelson, L.; Linke, H.; Borgström, M. Semiconductor Nanowire Array for Transparent Photovoltaic Applications. *Appl. Phys. Lett.* **2021**, *118*, 191107. [CrossRef]
9. Li, X.; Liu, X.; Li, Y.; Gao, D.; Cao, L. Using Novel Semiconductor Features to Construct Advanced ZnO Nanowires-Based Ultraviolet Photodetectors: A Brief Review. *IEEE Access* **2021**, *9*, 11954–11973. [CrossRef]
10. Dasgupta, N.P.; Sun, J.; Liu, C.; Brittman, S.; Andrews, S.C.; Lim, J.; Gao, H.; Yan, R.; Yang, P. 25th Anniversary Article: Semiconductor Nanowires—Synthesis, Characterization, and Applications. *Adv. Mater.* **2014**, *26*, 2137–2184. [CrossRef]
11. Seifert, W.; Borgström, M.; Deppert, K.; Dick, K.A.; Johansson, J.; Larsson, M.W.; Mårtensson, T.; Sköld, N.; Patrik, T.; Svensson, C.; et al. Growth of One-Dimensional Nanostructures in MOVPE. *J. Cryst. Growth* **2004**, *272*, 211–220. [CrossRef]
12. Hersee, S.D.; Sun, X.; Wang, X. The Controlled Growth of GaN Nanowires. *Nano Lett.* **2006**, *6*, 1808–1811. [CrossRef] [PubMed]
13. Wang, N.; Cai, Y.; Zhang, R.Q. Growth of Nanowires. *Mater. Sci. Eng. R Rep.* **2008**, *60*, 1–51. [CrossRef]
14. Vanmaekelbergh, D.; van Vugt, L.K. ZnO Nanowire Lasers. *Nanoscale* **2011**, *3*, 2783. [CrossRef]
15. Duan, X.; Huang, Y.; Agarwal, R.; Lieber, C.M. Single-Nanowire Electrically Driven Lasers. *Nature* **2003**, *421*, 241–245. [CrossRef]
16. Johnson, J.C.; Choi, H.-J.; Knutsen, K.P.; Schaller, R.D.; Yang, P.; Saykally, R.J. Single Gallium Nitride Nanowire Lasers. *Nat. Mater.* **2002**, *1*, 106–110. [CrossRef] [PubMed]
17. Saxena, D.; Mokkapati, S.; Parkinson, P.; Jiang, N.; Gao, Q.; Tan, H.H.; Jagadish, C. Optically Pumped Room-Temperature GaAs Nanowire Lasers. *Nat. Photonics* **2013**, *7*, 963–968. [CrossRef]
18. Zhu, H.; Fu, Y.; Meng, F.; Wu, X.; Gong, Z.; Ding, Q.; Gustafsson, M.V.; Trinh, M.T.; Jin, S.; Zhu, X.-Y. Lead Halide Perovskite Nanowire Lasers with Low Lasing Thresholds and High Quality Factors. *Nat. Mater.* **2015**, *14*, 636–642. [CrossRef]
19. Peng, K.; Jevtics, D.; Zhang, F.; Sterzl, S.; Damry, D.A.; Rothmann, M.U.; Guilhabert, B.; Strain, M.J.; Tan, H.H.; Herz, L.M.; et al. Three-Dimensional Cross-Nanowire Networks Recover Full Terahertz State. *Science* **2020**, *368*, 510–513. [CrossRef]
20. Zhang, A.; Zheng, G. Semiconductor Nanowires for Biosensors. In *Semiconductor Nanowires*; Elsevier: Amsterdam, The Netherlands, 2015; pp. 471–490. [CrossRef]
21. Li, H.; Li, D.; Chen, H.; Yue, X.; Fan, K.; Dong, L.; Wang, G. Application of Silicon Nanowire Field Effect Transistor (SiNW-FET) Biosensor with High Sensitivity. *Sensors* **2023**, *23*, 6808. [CrossRef]
22. Krajczewski, J.; Michałowska, A.; Čtvrtlík, R.; Nožka, L.; Tomáštík, J.; Václavek, L.; Turczyniak-Surdacka, S.; Bieńskowski, K.; Solarska, R. The Battle for the Future of SERS—TiN vs. Au Thin Films with the Same Morphology. *Appl. Surf. Sci.* **2023**, *618*, 156703. [CrossRef]
23. Otto, A. Excitation of Nonradiative Surface Plasma Waves in Silver by the Method of Frustrated Total Reflection. *Zeitschrift für Phys. A Hadron. Nucl.* **1968**, *216*, 398–410. [CrossRef]
24. Kretschmann, E.; Raether, H. Notizen: Radiative Decay of Non Radiative Surface Plasmons Excited by Light. *Zeitschrift für Naturforsch. A* **1968**, *23*, 2135–2136. [CrossRef]
25. Turkevich, J.; Stevenson, P.C.; Hillier, J. A Study of the Nucleation and Growth Processes in the Synthesis of Colloidal Gold. *Discuss. Faraday Soc.* **1951**, *11*, 55. [CrossRef]
26. Turkevich, J. Colloidal Gold. Part I. *Gold Bull.* **1985**, *18*, 86–91. [CrossRef]
27. Lee, P.C.; Meisel, D. Adsorption and Surface-Enhanced Raman of Dyes on Silver and Gold Sols. *J. Phys. Chem.* **1982**, *86*, 3391–3395. [CrossRef]
28. Langille, M.R.; Personick, M.L.; Zhang, J.; Mirkin, C.A. Defining Rules for the Shape Evolution of Gold Nanoparticles. *J. Am. Chem. Soc.* **2012**, *134*, 14542–14554. [CrossRef]
29. Wu, H.-L.; Chen, C.-H.; Huang, M.H. Seed-Mediated Synthesis of Branched Gold Nanocrystals Derived from the Side Growth of Pentagonal Bipyramids and the Formation of Gold Nanostars. *Chem. Mater.* **2009**, *21*, 110–114. [CrossRef]
30. Nikoobakht, B.; El-Sayed, M.A. Preparation and Growth Mechanism of Gold Nanorods (NRs) Using Seed-Mediated Growth Method. *Chem. Mater.* **2003**, *15*, 1957–1962. [CrossRef]
31. Burrows, N.D.; Harvey, S.; Idesis, F.A.; Murphy, C.J. Understanding the Seed-Mediated Growth of Gold Nanorods through a Fractional Factorial Design of Experiments. *Langmuir* **2017**, *33*, 1891–1907. [CrossRef]

32. Scarabelli, L.; Coronado-Puchau, M.; Giner-Casares, J.J.; Langer, J.; Liz-Marzán, L.M. Monodisperse Gold Nanotriangles: Size Control, Large-Scale Self-Assembly, and Performance in Surface-Enhanced Raman Scattering. *ACS Nano* **2014**, *8*, 5833–5842. [CrossRef]
33. Sun, Z.; Umar, A.; Zeng, J.; Luo, X.; Song, L.; Zhang, Z.; Chen, Z.; Li, J.; Su, F.; Huang, Y. Highly Pure Gold Nanotriangles with Almost 100% Yield for Surface-Enhanced Raman Scattering. *ACS Appl. Nano Mater.* **2022**, *5*, 1220–1231. [CrossRef]
34. Kou, X.; Ni, W.; Tsung, C.-K.; Chan, K.; Lin, H.-Q.; Stucky, G.D.; Wang, J. Growth of Gold Bipyramids with Improved Yield and Their Curvature-Directed Oxidation. *Small* **2007**, *3*, 2103–2113. [CrossRef] [PubMed]
35. Dovgolevsky, E.; Haick, H. Direct Observation of the Transition Point Between Quasi-Spherical and Cubic Nanoparticles in a Two-Step Seed-Mediated Growth Method. *Small* **2008**, *4*, 2059–2066. [CrossRef]
36. Zhang, J.; Langille, M.R.; Personick, M.L.; Zhang, K.; Li, S.; Mirkin, C.A. Concave Cubic Gold Nanocrystals with High-Index Facets. *J. Am. Chem. Soc.* **2010**, *132*, 14012–14014. [CrossRef]
37. Wiley, B.; Herricks, T.; Sun, Y.; Xia, Y. Polyol Synthesis of Silver Nanoparticles: Use of Chloride and Oxygen to Promote the Formation of Single-Crystal, Truncated Cubes and Tetrahedrons. *Nano Lett.* **2004**, *4*, 1733–1739. [CrossRef]
38. Zhao, T.; Sun, R.; Yu, S.; Zhang, Z.; Zhou, L.; Huang, H.; Du, R. Size-Controlled Preparation of Silver Nanoparticles by a Modified Polyol Method. *Colloids Surf. A Physicochem. Eng. Asp.* **2010**, *366*, 197–202. [CrossRef]
39. Callegari, A.; Tonti, D.; Chergui, M. Photochemically Grown Silver Nanoparticles with Wavelength-Controlled Size and Shape. *Nano Lett.* **2003**, *3*, 1565–1568. [CrossRef]
40. Yin, B.; Ma, H.; Wang, S.; Chen, S. Electrochemical Synthesis of Silver Nanoparticles under Protection of Poly(N-Vinylpyrrolidone). *J. Phys. Chem. B* **2003**, *107*, 8898–8904. [CrossRef]
41. Rodríguez-Sánchez, L.; Blanco, M.C.; López-Quintela, M.A. Electrochemical Synthesis of Silver Nanoparticles. *J. Phys. Chem. B* **2000**, *104*, 9683–9688. [CrossRef]
42. Tsuji, T.; Iryo, K.; Watanabe, N.; Tsuji, M. Preparation of Silver Nanoparticles by Laser Ablation in Solution: Influence of Laser Wavelength on Particle Size. *Appl. Surf. Sci.* **2002**, *202*, 80–85. [CrossRef]
43. Mafuné, F.; Kohno, J.; Takeda, Y.; Kondow, T.; Sawabe, H. Formation of Gold Nanoparticles by Laser Ablation in Aqueous Solution of Surfactant. *J. Phys. Chem. B* **2001**, *105*, 5114–5120. [CrossRef]
44. Kołątaj, K.; Ambroziak, R.; Kędziora, M.; Krajczewski, J.; Kudelski, A. Formation of Bifunctional Conglomerates Composed of Magnetic γ-Fe_2O_3 Nanoparticles and Various Noble Metal Nanostructures. *Appl. Surf. Sci.* **2019**, *470*, 970–978. [CrossRef]
45. Fujiwara, K.; Kasaya, H.; Ogawa, N. Gold Nanoparticle Monolayer Formation on a Chemically Modified Glass Surface. *Anal. Sci.* **2009**, *25*, 241–248. [CrossRef] [PubMed]
46. Kambayashi, M.; Zhang, J.; Oyama, M. Crystal Growth of Gold Nanoparticles on Indium Tin Oxides in the Absence and Presence of 3-Mercaptopropyl-Trimethoxysilane. *Cryst. Growth Des.* **2005**, *5*, 81–84. [CrossRef]
47. Kim, K.; Lee, J.W.; Lee, H.B.; Shin, K.S. Novel Fabrication of Au Nanoparticle Films on Planar and Curved Surfaces of Glass and Fiber Materials. *Langmuir* **2009**, *25*, 9697–9702. [CrossRef]
48. Jiang, Y.; Lu, Y.; Zhang, L.; Liu, L.; Dai, Y.; Wang, W. Preparation and Characterization of Silver Nanoparticles Immobilized on Multi-Walled Carbon Nanotubes by Poly(Dopamine) Functionalization. *J. Nanoparticle Res.* **2012**, *14*, 938. [CrossRef]
49. Spampinato, V.; Parracino, M.A.; La Spina, R.; Rossi, F.; Ceccone, G. Surface Analysis of Gold Nanoparticles Functionalized with Thiol-Modified Glucose SAMs for Biosensor Applications. *Front. Chem.* **2016**, *4*, 8. [CrossRef]
50. Ambroziak, R.; Krajczewski, J.; Pisarek, M.; Kudelski, A. Immobilization of Cubic Silver Plasmonic Nanoparticles on TiO_2 Nanotubes, Reducing the Coffee Ring Effect in Surface-Enhanced Raman Spectroscopy Applications. *ACS Omega* **2020**, *5*, 13963–13972. [CrossRef]
51. Krajczewski, J.; Ambroziak, R.; Turczyniak-Surdacka, S.; Dziubałtowska, M. WO_3 Nanopores Array Modified by Au Trisoctahedral NPs: Formation, Characterization and SERS Application. *Materials* **2022**, *15*, 8706. [CrossRef]
52. Laurenčíková, A.; Eliáš, P.; Hasenöhrl, S.; Kováč, J.; Szobolovszký, R.; Novák, J. GaP nanocones covered with silver nanoparticles for surface-enhanced Raman spectroscopy. *Appl. Surf. Sci.* **2018**, *461*, 149–159. [CrossRef]
53. Novák, J.; Eliáš, P.; Hasenöhrl, S.; Laurenčíková, A.; Kováč, J.; Urbancovám, P.; Pudiš, D. Twinned nanoparticle structures for surface enhanced Raman scattering. *Appl. Surf. Sci.* **2020**, *528*, 146548. [CrossRef]
54. Novák, J.; Laurenčíková, A.; Eliáš, P.; Hasenöhrl, S.; Sojková, M.; Dobrocka, E.; Kováč, J.; Kováč, J.; Ďurišová, J.; Pudiš, D. Nanorods and nanocones for advanced sensor applications. *Appl. Surf. Sci.* **2018**, *461*, 61–65. [CrossRef]
55. Chien, F.-C.; Zhang, T.F.; Chen, C.; Nguyet Nguyen, T.A.; Wang, S.-Y.; Lai, S.M.; Cin, C.H.; Huang, C.-K.; Liu, C.-Y.; Lai, K.Y. Nanostructured InGaN Quantum Wells as a Surface-Enhanced Raman Scattering Substrate with Expanded Hot Spots. *ACS Appl. Nano Mater.* **2021**, *4*, 2614–2620. [CrossRef]
56. Helmersson, U.; Lattemann, M.; Bohlmark, J.; Ehiasarian, A.P.; Gudmundsson, J.T. Ionized Physical Vapor Deposition (IPVD): A Review of Technology and Applications. *Thin Solid Film.* **2006**, *513*, 1–24. [CrossRef]
57. Hong, C.; Kim, H.; Park, S.; Lee, C. Optical Properties of Porous Silicon Coated with Ultrathin Gold Film by RF-Magnetron Sputtering. *J. Eur. Ceram. Soc.* **2010**, *30*, 459–463. [CrossRef]
58. Uosaki, K.; Shen, Y.; Kondo, T. Preparation of a Highly Ordered Au (111) Phase on a Polycrystalline Gold Substrate by Vacuum Deposition and Its Characterization by XRD, GISXRD, STM/AFM, and Electrochemical Measurements. *J. Phys. Chem.* **1995**, *99*, 14117–14122. [CrossRef]

59. Barman, T.; Nozka, L.; Prochazka, V.; Michałowska, A.; Turczyniak-Surdacka, S.; Ctvrtlik, R.; Krajczewski, J. Morphology Tuned Plasmonic TiN Nanostructures Formed by Angle-Dependent Sputtering Process for SERS Measurements. *J. Mater. Sci.* **2023**, *58*, 14661–14672. [CrossRef]
60. Krajczewski, J.; Dumiszewska, E.; Czolak, D.; Turczyniak Surdacka, S.; Kudelski, A. New, Epitaxial Approach to SERS Platform Preparation—InP Nanowires Coated by an Au Layer as a New, Highly Active, and Stable SERS Platform. *Appl. Surf. Sci.* **2023**, *607*, 155096. [CrossRef]
61. Kudelski, A. Surface-Enhanced Raman Scattering Study of Monolayers Formed from Mixtures of 4-Mercaptobenzoic Acid and Various Aromatic Mercapto-Derivative Bases. *J. Raman Spectrosc.* **2009**, *40*, 2037–2043. [CrossRef]
62. Carlsson, J.-O.; Martin, P.M. Chemical Vapor Deposition. In *Handbook of Deposition Technologies for Films and Coatings*; Elsevier: Amsterdam, The Netherlands, 2010; pp. 314–363. [CrossRef]
63. O'Brien, P. Chemical Vapor Deposition. In *Encyclopedia of Materials: Science and Technology*; Elsevier: Amsterdam, The Netherlands, 2001; pp. 1173–1176. [CrossRef]
64. Sun, X.; Li, H. Gold Nanoisland Arrays by Repeated Deposition and Post-Deposition Annealing for Surface-Enhanced Raman Spectroscopy. *Nanotechnology* **2013**, *24*, 355706. [CrossRef]
65. Araújo, A.; Mendes, M.J.; Mateus, T.; Vicente, A.; Nunes, D.; Calmeiro, T.; Fortunato, E.; Águas, H.; Martins, R. Influence of the Substrate on the Morphology of Self-Assembled Silver Nanoparticles by Rapid Thermal Annealing. *J. Phys. Chem. C* **2016**, *120*, 18235–18242. [CrossRef]
66. Berger, L.-M. Application of Hardmetals as Thermal Spray Coatings. *Int. J. Refract. Met. Hard Mater.* **2015**, *49*, 350–364. [CrossRef]
67. Naik, G.V.; Schroeder, J.L.; Ni, X.; Kildishev, A.V.; Sands, T.D.; Boltasseva, A. Titanium Nitride as a Plasmonic Material for Visible and Near-Infrared Wavelengths. *Opt. Mater. Express* **2012**, *2*, 478. [CrossRef]
68. Jen, Y.-J.; Lin, M.-J.; Cheang, H.-L.; Chan, T.-L. Obliquely Deposited Titanium Nitride Nanorod Arrays as Surface-Enhanced Raman Scattering Substrates. *Sensors* **2019**, *19*, 4765. [CrossRef]
69. Kaisar, N.; Huang, Y.-T.; Jou, S.; Kuo, H.-F.; Huang, B.-R.; Chen, C.-C.; Hsieh, Y.-F.; Chung, Y.-C. Surface-Enhanced Raman Scattering Substrates of Flat and Wrinkly Titanium Nitride Thin Films by Sputter Deposition. *Surf. Coat. Technol.* **2018**, *337*, 434–438. [CrossRef]
70. Zhao, F.; Xue, X.; Fu, W.; Liu, Y.; Ling, Y.; Zhang, Z. TiN Nanorods as Effective Substrate for Surface-Enhanced Raman Scattering. *J. Phys. Chem. C* **2019**, *123*, 29353–29359. [CrossRef]
71. Mascaretti, L.; Barman, T.; Bricchi, B.R.; Münz, F.; Li Bassi, A.; Kment, Š.; Naldoni, A. Controlling the Plasmonic Properties of Titanium Nitride Thin Films by Radiofrequency Substrate Biasing in Magnetron Sputtering. *Appl. Surf. Sci.* **2021**, *554*, 149543. [CrossRef]
72. Guler, U.; Suslov, S.; Kildishev, A.V.; Boltasseva, A.; Shalaev, V.M. Colloidal Plasmonic Titanium Nitride Nanoparticles: Properties and Applications. *Nanophotonics* **2015**, *4*, 269–276. [CrossRef]
73. Guler, U.; Zemlyanov, D.; Kim, J.; Wang, Z.; Chandrasekar, R.; Meng, X.; Stach, E.; Kildishev, A.V.; Shalaev, V.M.; Boltasseva, A. Plasmonic Titanium Nitride Nanostructures via Nitridation of Nanopatterned Titanium Dioxide. *Adv. Opt. Mater.* **2017**, *5*, 1600717. [CrossRef]
74. Wei, H.; Wu, M.; Dong, Z.; Chen, Y.; Bu, J.; Lin, J.; Yu, Y.; Wei, Y.; Cui, Y.; Wang, R. Composition, Microstructure and SERS Properties of Titanium Nitride Thin Film Prepared via Nitridation of Sol-Gel Derived Titania Thin Films. *J. Raman Spectrosc.* **2017**, *48*, 578–585. [CrossRef]
75. Kan, X.; Deng, C.; Yu, C.; Ding, J.; Zhu, H. Synthesis, Electrochemical and Photoluminescence Properties of Titanium Nitride Nanoparticles. *J. Mater. Sci. Mater. Electron.* **2018**, *29*, 10624–10630. [CrossRef]
76. Xia, F.; Yang, A.; Cui, W.; Li, Q. Preparation and Wear Assessment of Ultrasonic Electrodeposited Ni–TiN Thin Films. *Ceram. Int.* **2018**, *44*, 11070–11076. [CrossRef]
77. Wu, H.; Wang, H.; Li, G. Metal Oxide Semiconductor SERS-Active Substrates by Defect Engineering. *Analyst* **2017**, *142*, 326–335. [CrossRef]
78. Li, J.; Xu, X.; Huang, B.; Lou, Z.; Li, B. Light-Induced In Situ Formation of a Nonmetallic Plasmonic MoS_2 /MoO_{3-x} Heterostructure with Efficient Charge Transfer for CO_2 Reduction and SERS Detection. *ACS Appl. Mater. Interfaces* **2021**, *13*, 10047–10053. [CrossRef] [PubMed]
79. Patil, M.K.; Gaikwad, S.H.; Mukherjee, S.P. Phase- and Morphology-Controlled Synthesis of Tunable Plasmonic MoO_{3-x} Nanomaterials for Ultrasensitive Surface-Enhanced Raman Spectroscopy Detection. *J. Phys. Chem. C* **2020**, *124*, 21082–21093. [CrossRef]
80. He, R.; Lai, H.; Wang, S.; Chen, T.; Xie, F.; Chen, Q.; Liu, P.; Chen, J.; Xie, W. Few-Layered VdW MoO3 for Sensitive, Uniform and Stable SERS Applications. *Appl. Surf. Sci.* **2020**, *507*, 145116. [CrossRef]
81. Yang, Y.; Li, J.; Zhang, M.; Song, P.; Lu, X.; Ding, Y. Universal and Simple MoO_3 Substrate for Identification of SERS Enhancement Mechanism. *J. Raman Spectrosc.* **2021**, *52*, 1275–1280. [CrossRef]
82. Kulikova, D.P.; Dobronosova, A.A.; Kornienko, V.V.; Nechepurenko, I.A.; Baburin, A.S.; Sergeev, E.V.; Lotkov, E.S.; Rodionov, I.A.; Baryshev, A.V.; Dorofeenko, A.V. Optical properties of tungsten trioxide, palladium, and platinum thin films for functional nanostructures engineering. *Opt. Express.* **2020**, *28*, 32049–32060. [CrossRef] [PubMed]
83. Jiang, L.; Hu, Y.; Zhang, H.; Luo, X.; Yuan, R.; Yang, X. Charge-Transfer Resonance and Surface Defect-Dominated WO_3 Hollow Microspheres as SERS Substrates for the MiRNA 155 Assay. *Anal. Chem.* **2022**, *94*, 6967–6975. [CrossRef]

84. Shi, Y.; Liu, Q.; Hong, R.; Tao, C.; Wang, Q.; Lin, H.; Han, Z.; Zhang, D. SERS-Active WO_{3-x} Thin Films with Tunable Surface Plasmon Resonance Induced by Defects from Thermal Treatment. *Spectrochim. Acta Part A Mol. Biomol. Spectrosc.* **2022**, *268*, 120686. [CrossRef]
85. Hou, X.; Luo, X.; Fan, X.; Peng, Z.; Qiu, T. Plasmon-Coupled Charge Transfer in WO_{3-x} Semiconductor Nanoarrays: Toward Highly Uniform Silver-Comparable SERS Platforms. *Phys. Chem. Chem. Phys.* **2019**, *21*, 2611–2618. [CrossRef] [PubMed]
86. Riswana Barveen, N.; Wang, T.-J.; Chang, Y.-H.; Rajakumaran, R. Ultrasensitive and Reusable SERS Platform Based on Ag Modified WO_3 Nanoflakes for Catechol Detection. *Mater. Sci. Eng. B* **2022**, *282*, 115753. [CrossRef]
87. Zou, J.-W.; Li, Z.-D.; Kang, H.-S.; Zhao, W.-Q.; Liu, J.-C.; Chen, Y.-L.; Ma, L.; Hou, H.-Y.; Ding, S.-J. Strong Visible Light Absorption and Abundant Hotspots in Au-Decorated WO_3 Nanobricks for Efficient SERS and Photocatalysis. *ACS Omega* **2021**, *6*, 28347–28355. [CrossRef] [PubMed]
88. Juntaracena, K.; Yuangkaew, T.; Horprathum, M.; Triroj, N.; Jaroenapibal, P. Surface-Enhanced Raman Scattering Activities and Recyclability of Ag-Incorporated WO_3 Nanofiber-Based Substrates. *Vib. Spectrosc.* **2021**, *115*, 103276. [CrossRef]